



Nanoscale

**Cell mechanics can be robustly derived from AFM indentation data using brush model: error analysis**

Journal:	<i>Nanoscale</i>
Manuscript ID	NR-ART-01-2022-000041.R1
Article Type:	Paper
Date Submitted by the Author:	21-Feb-2022
Complete List of Authors:	Makarova, Nadezda; Tufts University School of Engineering Sokolov, Igor; Tufts University School of Engineering

SCHOLARONE™  
Manuscripts

# Cell mechanics can be robustly derived from AFM indentation data using brush model: error analysis

*N. Makarova<sup>1</sup>, I. Sokolov<sup>1,2,3</sup>\**

<sup>1</sup>Department of Mechanical Engineering, <sup>2</sup>Department of Biomedical Engineering, <sup>3</sup> Department of Physics, Tufts University, Medford, MA, USA

E-mail of the corresponding author: igor.sokolov@tufts.edu

## Abstract

The brush model was introduced to interpret AFM indentation data collected on biological cells in a more consistent way compared just to the traditional Hertz model. It takes into account the presence of non-Hertzian deformation of the pericellular brush-like layer surrounding cells (a mix of glycocalyx molecules and microvilli/microridges). The model allows finding the effective Young's modulus of the cell body in a less depth-dependent manner. In addition, it allows to find the force due to the pericellular brush layer. Compared to simple mechanical models used to interpret the indentation experiments, the brush model has additional complexity. It raises the concern about the possible unambiguity of separation of mechanical properties of the cell body and pericellular layer. Here we present the analysis of the robustness of the brush model and demonstrate a weak dependence of the obtained results on the uncertainties within the model and experimental data. We critically analyzed the use of the brush model on a variety of AFM force curves collected on rather distinct cell types: human cervical epithelial cells, rat neurons, and zebrafish melanocytes. We conclude that the brush model is robust; the errors in the definition of the effective Young's modulus due to possible uncertainties of the model and experimental data are within 4%, which is less than the error, for example, due to a typical uncertainty in the spring constant of the AFM cantilever. We also discuss the errors of parameterization of the force due to the pericellular brush layer.

## 1. Introduction

Atomic force microscopy (AFM) has shown the ability of high-resolution imaging of biological surfaces in situ and in vivo <sup>1-3</sup>. However, the true uniqueness of AFM is its capability to measure various physical and mechanical properties of sample surfaces. The study of cell mechanics by means of AFM is an active area of research <sup>4-6</sup>. Mechanical properties of cells are important factors that define cell functionality, motility, tissue formation <sup>7, 8</sup>, stem cell differentiation <sup>9</sup>, etc. Correlation between cell elasticity and various human diseases, abnormalities has been implicated in the pathogenesis of such diseases as vascular diseases, cancer, malaria, kidney disease, cataracts, Alzheimer's Dementia, complications of diabetes, cardiomyopathies, arthritis, and even aging <sup>10-12</sup>. The stiffening of red blood cells infected with malaria <sup>13, 14</sup> was found to be responsible for fatal incidents of this disease. Low rigidity of the majority of cancer cells was recently suggested to be used for cancer diagnosis <sup>15, 16</sup>. Therefore, besides the fundamental interest, there is a practical need to measure cell mechanics quantitatively.

It has recently been shown that the AFM indentation allows extracting information not only about cell mechanics but also about the pericellular coat or brush-like layer surrounding eukaryotic and the majority of prokaryotic cells <sup>5, 6, 17, 18</sup>. The pericellular brush (**PB**) layer is a combination of glycosaccharides, glycoproteins, and membrane protrusions (microridges and microvilli). The biological significance of this layer is known though not fully investigated. It was demonstrated that damages of the PB layer led to multiple diseases and complications, such as cardiovascular and blood-related diseases <sup>19, 20</sup>, and the change in the invasiveness of cancer cells <sup>21-23</sup>. In particular, artificial removal of the molecular part of the PB layer enhances the ability of cells to move through tissue and increases the cell adhesion to the walls of blood vessels <sup>21, 22, 24</sup>. Furthermore, it was shown that this layer is substantially changed when cells become cancerous <sup>25</sup>. A whole series of works on AFM imaging of physical properties of the cell surface, which were performed on fixed dried cells, showed a substantial change of the cell surface during progression towards cancer <sup>26-29</sup>. It was demonstrated on the human cervical cancer model in vitro <sup>26-28</sup>, and recently, on cells extracted from urine of patients who have active bladder cancer (patients with no bladder cancer were the control group) <sup>30</sup>. Furthermore, the use of a novel AFM imaging mode, named Ringing mode, allowed to separate two similar cell lines

of human colorectal epithelial cancer of different aggressiveness based on the use of images of the cell surface <sup>31</sup>.

The brush model was suggested to find the effective Young's modulus of the cell body, which is covered with the PB layer, through the analysis of the force curves collected in AFM indentation experiments. The model takes into account the presence of the non-Hertzian behavior of the PB layer. As was demonstrated <sup>32</sup>, the brush model allowed extraction of the effective Young's modulus of the cell body in a self-consistent, nearly depth-independent manner. Without taking the brush layer into consideration, the effective Young's modulus of the cell typically shows a strong depth dependence <sup>4,33</sup>. It should be noted that it is still technically possible to use a "relative" modulus of elasticity and without the brush model, for example, to classify cells with substantially different elastic modulus. However, the lack of self-consistency of the used Hertz model creates a substantial difficulty in comparing the results obtained in different laboratories because it requires to verify the degree of deviation from the non-Hertzian behavior, which might be different in different experimental setups. Extraction of the force due to the PB layer is an important bonus of the brush model. When analyzing the obtained force dependence due to the PB layer, it was found that the PB layer could be reasonably described using the Alexander-de Gennes model, which is typically a good description of grafted polymer molecules or polymer brushes.

The brush model was experimentally verified on soft polymers covered with a small polymer brush <sup>34</sup>. The ability of the model to distinguish contributions of long polysaccharide molecules to the PB layer and the corrugations of the pericellular membrane (microridges and microvilli) was demonstrated using guinea pig fibroblast cells <sup>35</sup>. The utility of the brush model was confirmed in the study of cancer cells <sup>6,25,35-37</sup>, aging <sup>38</sup>, the dependence of cell mechanics on cell passages <sup>36</sup>, etc.

Despite the demonstration of the utility of the brush model, it has not been yet broadly used. Besides the additional complexity of the brush model, the robustness of the model was not investigated in a systematic way. It is paramount for any physical model to prove the model robustness <sup>39-41</sup>, i.e., stability of the obtained results against various uncertainties in the experimental data and possible ambiguities in the model.

Here we present a comprehensive analysis of the robustness of the brush model applied to the study of cells. We analyze the dependence of the accuracy of the extracted cell parameters (cell modulus and characteristics of the PB layer) on possible uncertainties within the model and experimental data. We use the AFM indentation data (force curves) obtained collected on cells from rather distinctive regions of the cell realm, human cervical epithelial cells, rat neurons, and zebrafish melanocytes. We show that the uncertainties in the calculation of the cell effective Young's modulus are small ( $<4\%$ ) across all three types of cells. It is worth noting that the obtained uncertainties/errors are substantially smaller than the well-known errors in the AFM indentation experiments, such as the uncertainty in the value of the spring constant of the AFM cantilever (5-20%) and the Poisson ratio of the cell material ( $\sim 5\%$ )<sup>4, 32, 42</sup>. We also discuss the variations of calculation of the brush parameters (the force-due-to-brush layer), which can be as high as 25% when attempting to fit in the Alexander - de Gennes model. It is important to stress that these variations are completely independent of the calculation of the effective Young's modulus of the cell body. Moreover, the variations of the brush parameters are conceivably real heterogeneity in the repulsive force within the PB layer. Thus, it can be informative by itself.

## **2. The brush model in brief and definitions of possible uncertainties in the brush model**

The brush model was described in detail in<sup>17, 32, 43, 44</sup>. Here we give a short description of the model while presenting details of its major steps. In particular, we describe specific steps of data processing within the brush model, which allow for some uncertainty in the interpretation of experimental data.

It should be noted that both the approach and retraction force curves are recorded during AFM indentation. However, only the approach curve is further used for the analysis because the AFM probe is known to disturb the PB layer of the cell, and it may have insufficient time to relax to contribute fully to the retraction curve. In other words, the retraction curve carries a signature of a complex dynamic of relaxation of the cell deformation, which is excessively complicated to be analyzed at this stage. Thus, the approach curve is a better representation of an undisturbed cell surface. We will not discuss the speed dependence on the force curves here. As

was shown in <sup>6</sup>, the brush model is applicable to the force curves in a large range of the indentation speeds. Obviously, the extracted effective Young's modulus can still only be called an *effective* Young's modulus because of heterogeneity of the cell material.

As was previously demonstrated, the brush model is self-consistent only when using a relatively dull AFM probe <sup>4, 32</sup>. The use of a standard commercial sharp probe presumably leads to a nonlinear overstretched response of cellular material <sup>45</sup>, which results in much higher and depth-dependent values of the modulus. Thus, only a large spherical AFM indenter will be considered here.

## 2.1. The brush model in brief

The brush model was introduced to take into account a “brushy” interface of biological cells, which consists of the corrugation of the pericellular membrane and glycocalyx molecules. Here we will not discuss the basic assumptions of this model because it is described in detail in the previous publications. But we review the steps we need to go through to analyze the indentation data with the brush model. This is needed to describe in the next Section 2.2 the places in which there are possible uncertainties in the processing of the data.

The force indentation curves collected by AFM are analyzed in two steps. During the 1<sup>st</sup> step, the model allows deriving an effective Young's modulus of the cell body that is relatively self-consistent with the assumption of homogeneous and isotropic approximation of the cell material. In the 2<sup>nd</sup> step, the model allows to extract the force due to the intrinsically nonlinear PB layer. The model deals with the processing of “raw” force-indentation curves collected in one of the vertical ramping (vertical oscillatory) modes, which can simultaneously record cell topography (for example, the classical force-volume mode). The raw data of the force curve means the data describing the dependency of the cantilever deflection  $d$  on the vertical displacement of the AFM scanner  $Z$ . An example of such a curve is shown in Fig. 1a. An AFM probe deforming a cell surface, which is covered with the PB layer, is also shown in Fig. 1a for different parts of the force curve. The origin of  $Z$  ( $Z=0$ ) is defined at the maximum deflection of the AFM cantilever (maximum indentation force that is typical for Bruker AFMs; this is not universal and has to be modified for other formats of AFM files). Simple geometrical reasoning gives the following relation between the geometrical parameters defined in Fig. 1b:

$$h = Z - Z_0 + i + d, \quad (1)$$

where  $Z_0$  is the position of the undeformed cell body,  $h$  is the distance between the AFM probe and the surface of the cell body,  $i$  is the deformation of the cell body. The latter can be calculated using the Hertz model:

$$i = \left[ \frac{9}{16} \frac{k}{E} \sqrt{\frac{R_{probe} + R_{cell}}{R_{probe} R_{cell}}} \right]^{2/3} d^{2/3}, \quad (2)$$

where  $E$  is the (effective) Young's modulus,  $k$  is the spring constant of the AFM cantilever, and  $R_{probe}$  ( $R_{cell}$ ) are the radius of the AFM probe (cell). The Poisson ratio of a cell is chosen to be 0.5 (because of a small range of possible variations of  $\nu$ , the error in the modulus due to the uncertainty of its definition is relatively small, within 5%<sup>32</sup>).

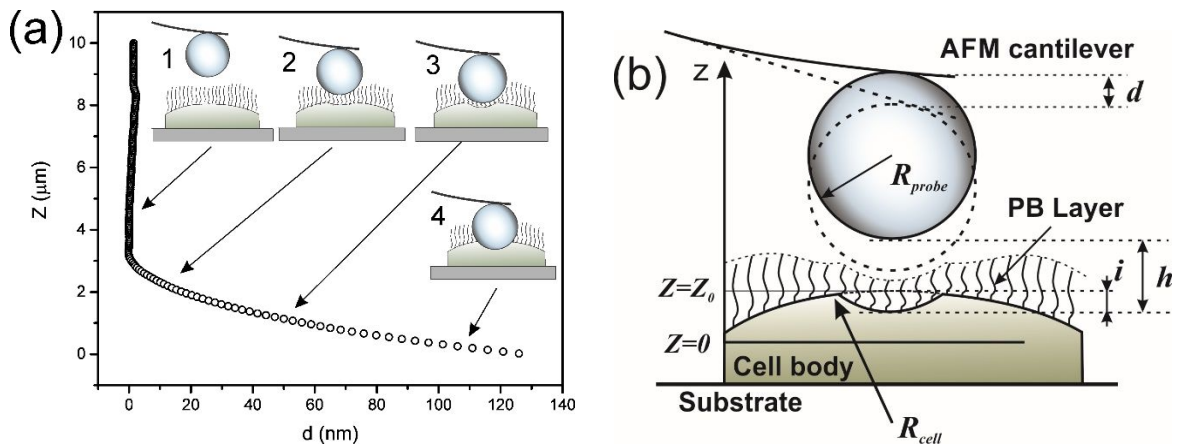


**Figure 1.** (a) An example of raw force curve, showing the different positions of the AFM probe and deformation of the cell body/PB layer. (b) A schematic of interaction between an AFM spherical indenter (probe) and cell demonstrating definitions of the parameters used in the brush model.  $Z$  is the vertical position of the AFM scanner,  $d$  is the cantilever deflection,  $Z_0$  is the undeformed position of the cell body,  $i$  is the deformation of the cell body,  $Z=0$  is at the maximum deflection (assigned by the AFM user), and  $h$  is the separation between the cell body and AFM probe.

Within the brush model, raw data obtained from the indentation experiments ( $Z$  versus  $d$ ) are processed in two steps. These steps are described below and also presented in a schematic shown in Figure 2.

**Step 1:** Finding the (effective) Young's modulus of the cell body. The whole concept of the Young's modulus is based on the assumption of isotropy and homogeneity of the sample material. While isotropy could be considered to be a good approximation for a majority of cells (unless they are elongated with explicitly anisotropic stress fibers), cells are obviously far from being homogeneous. Nonetheless, it is well-known that even a highly heterogeneous material can be treated as approximately homogeneous for sufficiently small stresses/strains. Sufficiently large forces would allow AFM to start detecting the inhomogeneity, for example, due to the internal structure of cells, organelles, and even typically rigid substrate. Therefore, the indentation force should not be too large to avoid the heterogeneity problem. To find such forces, it was suggested to use the strong linearity principle (see, e.g., <sup>44</sup> for detail), which stands that the obtained effective Young's modulus should be independent of the indentation depth (or the load force). It is the necessary condition of applicability of the Hertz model <sup>46</sup>. The Hertz model is chosen because of the use of a spherical indenter, approximately spherical cell contact, and negligible adhesion between the probe and cell surface (the adhesion is typically either absent or small compared to the indenting force). Thus, one needs to find a limit of the load force, above which the modulus is no longer constant.

On the other hand, due to the presence of the PB layer, the attempts to use very small force have failed to provide the depth independent effective Young's modulus either <sup>6,44</sup>. It was shown that this pericellular layer behaves quite similar to the polymeric brushes, which is characterized by the exponential force dependence between the probe and the grafted polymer brush (see, Step 2, eq. 2). Because of highly nonlinear behavior, the PB layer cannot be reasonably approximated as an elastic material. The brush model operates in the assumption that the PB layer is softer than the cell body. As a result, the AFM probe squeezes the PB layer much faster than deforms the cell body. At one point the stiffness of the squeezed PB layer becomes equal to the stiffness of the cell body. After that one can analyze the elastic properties of the cell body, and search for the independence of the effective Young's modulus of the indentation depth. Thus, the indentation force should be not too small to avoid highly nonlinear contribution to the indentation force curve from the PB layer.

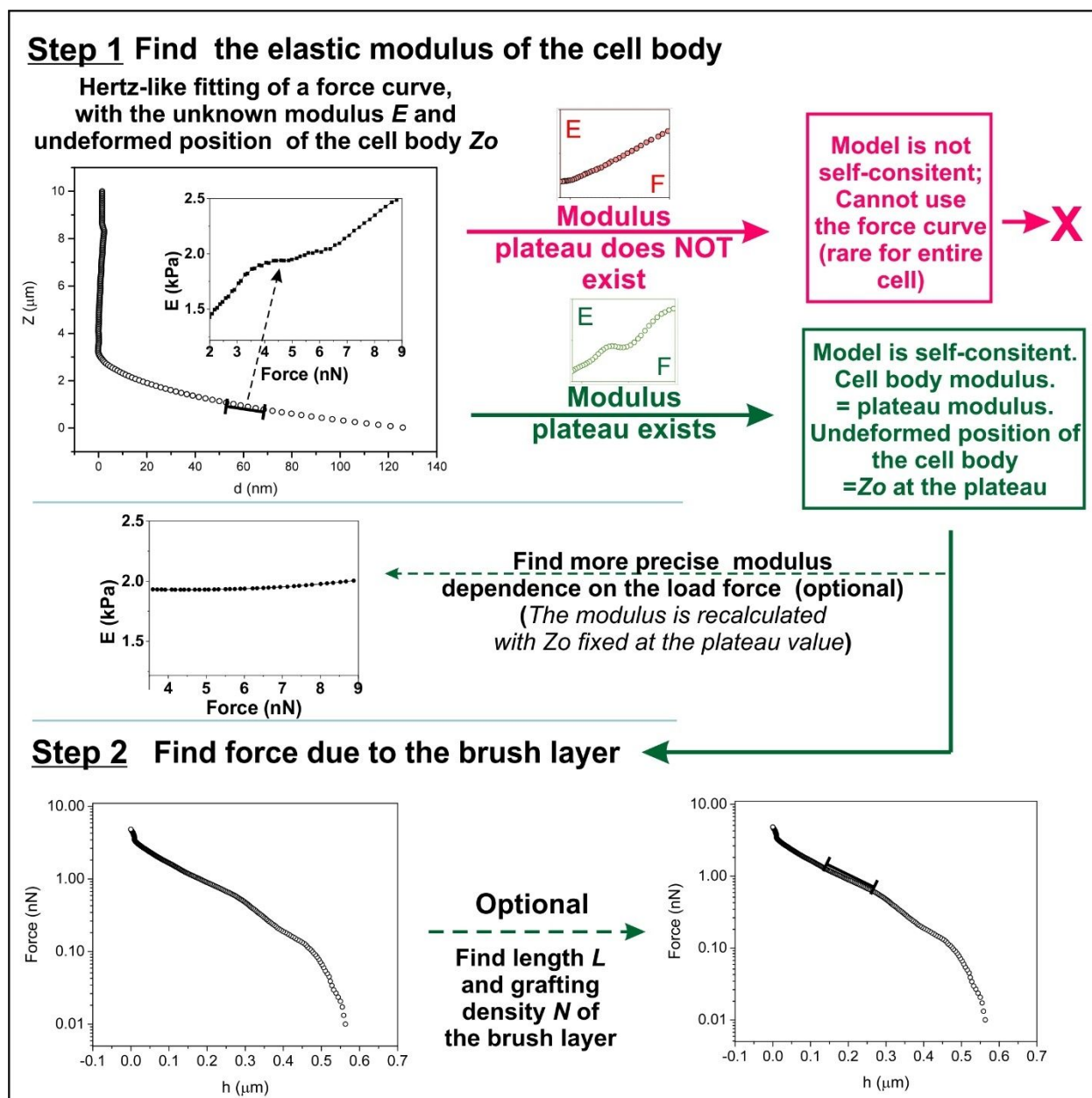


**Figure 2.** An example of processing raw indentation AFM data through the brush model. Step 1 shows the fitting which defines the effective Young's modulus of the cell body (the values of the modulus at the depth-independent plateau). An optional step allows deriving more precise modulus dependence on the load force by fixing  $Z_0$  (undeformed position of the cell body). Step 2 displays the derived force due to the PB layer at the function of the distance between the AFM probe and cell surface. One can typically see the exponential force dependence (straight line in the logarithmic force scale). Optionally, one can find the length and grafting density of the PB layer using equation (2).

Thus, the first step of the brush model is to find the region of the force indentation curve, in which the indentation force is sufficiently large to substantially squeeze the PB layer and not too large to start detecting heterogeneity of the cell and its substrate. As described above, to find this appropriate range of forces, one should analyze the dependence of the modulus on the indentation depth. The Young's modulus is determined from the fit of this part of the indentation force curve by using equation (1) in which  $h=0$ . In addition to the Young's modulus, each fitting interval gives the unknown undeformed position of the cell body  $Z_0$ . The appropriate force range should correspond to a plateau in the modulus dependence as a function of the indentation depth. Examples of the modulus plateau are shown in Figures 2, 3, 5. Quantitatively, a plateau was defined by a tilt less than 10%, using the least-square fit over the tested force range. Fortunately, the plateau seems to exist for virtually all cells.

It is worth noting that although we treat  $Z_0$  as a free fitting parameter, the undeformed position of the cell body is unique; it cannot change for different indentation forces by definition. We found that if one fixes  $Z_0$  and its value in the middle of the plateau and considers the Young's modulus as the only unknown parameter in the above fitting, the plateau is substantially increasing. It is clear that the value of the modulus will not change compared to the value of the plateau. Therefore, this procedure makes sense if one obtains a relatively flat dependence of the Young's modulus on the indentation depth/force. Figure 3 shows an example of such processing of a force curve. The modulus is recalculated for each part of the force curve (eq. 1 with  $h=0$ ) while keeping  $Z_0$  fixed at the value of the plateau. Because of the assumption of the squeezed brush when calculating the modulus ( $h=0$ ), this step cannot be directly applied to the forces smaller than the minimum force of plateau when the PB layer is not squeezed (nevertheless, it is possible to estimate the modulus for those small forces by characterizing out the force due to brush, see ref.<sup>32</sup> for detail).

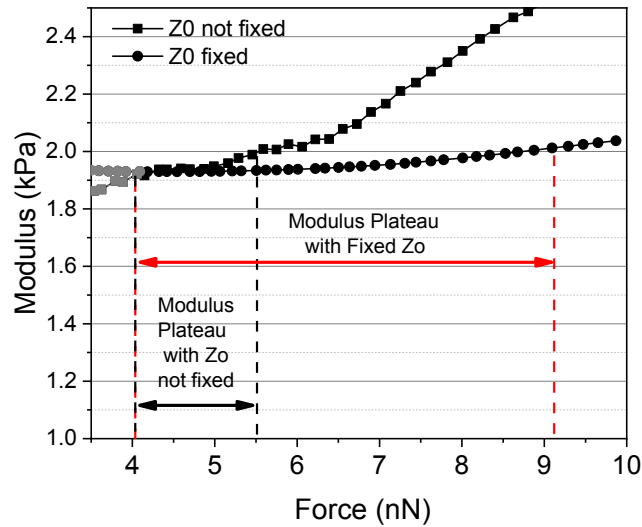


**Figure 3.** An example of dependence of the Young's modulus on the indentation depth/force. The modulus is found by fitting the experimental data using two approaches when treating  $Z_0$  is a fitting parameter and when it is fixed. The plateau is substantially increased when  $Z_0$  is fixed.

**Step 2:** Finding the force due to the pericellular brush layer; parameterization of this layer with the effective grafting density and brush length. The force due to the presence of the PB layer,  $F(h) = k \cdot d(h)$ , is extracted from the experimental data by treating equation (1) as the equation for the inverse function,  $h(d)$ . It is calculated while keeping  $E$  and  $Z_0$  fixed at the plateau values found in Step 1. Up to this point, the force extracted due to the PB layer is unambiguous up to the parameters  $E$  and  $Z_0$  obtained in the previous step. Fig.2 shows an example of such force extracted from the raw indentation data shown in the same figure.

As an optional step, one can characterize the force due to the PB layer with just two physical parameters. Besides getting some hint about the physical nature of the observed force, it is also useful to do for the convenience of comparison different PB layers. For example, we have suggested to use an exponential force dependence, which is typically observed when indenting an entropic polymeric brush layer. The validity of the exponential approximation can typically be seen if one plots the force due to the PB layer in the logarithmic scale (shown in Figure 2, Step 2). A clear straight line in such a plot indicates the exponential force-distance dependence. To

describe the parameters of such a layer, the following equation (Alexander - de Gennes model) is used for the force of repulsion between a spherical probe of radius  $R_{probe}$  and a semi-spherical cell of radius  $R_{cell}$ <sup>18, 47, 48</sup>:

$$F(h) \approx 100k_B T R^* N^{3/2} \exp\left(-2\pi \frac{h}{L}\right) L, \quad (2)$$

where  $k_B$  is the Boltzmann constant,  $T$  is the temperature,  $R^* = R_{probe} \cdot R_{cell} / (R_{probe} + R_{cell})$ ,  $N$  is the surface density of the brush constituents (grafting density, or effective molecular density), and  $L$  is the equilibrium thickness of the brush layer. Note that this formula is valid provided  $0.1 < h/L < 0.8$ .

## 2.2. Possible uncertainties in the brush model

Here we define possible uncertainties in the brush model and experimental data by exemplifying the application of the brush model in detail to calculate corresponding errors in finding the effective Young's modulus of the cell body (Step 1) and parameters of the PB layer (Step 2).

### 2.2.1. Possible errors due to uncertainty in the measured zero deflection of the AFM cantilever (zero force)

An example of a well-defined zero force before the probe starts to interact with cells is shown in Fig. 4a. However, sometimes the force curve can demonstrate a different behavior before the contact. Fig. 4b shows an example of a possible uncertainty in the definition of zero deflection of the AFM cantilever before it touches the cell. One can see a sort of jump of the AFM probe in the vicinity of the cell (recall that the approach force curve is shown). In principle, the behavior shown in Fig. 4b seems to be visually similar to well-known jump-to-contact behavior, which could be interpreted as a strong attraction of the AFM probe to the pericellular layer.

Implementing adhesive effects into the fit would require a modification of Alexander - de Gennes model (eq. 1), which describes the interaction of a surface with a brush layer. To the best of our knowledge, such a modification does not exist. Secondly, the jump may be just an artifact of multiple reflections of coherent laser light used in the cantilever deflection measurements, which is a substantial problem of many AFM optical detection systems. Furthermore, the

specific behavior exemplified in Fig. 4b is not universal. So instead of analyzing the reason for such behavior, one can declare it as an uncertainty in the definition of zero deflection of the AFM cantilever (zero force).

The error due to this uncertainty can be found as follows. For example, the uncertainty of zero deflection of the AFM cantilever shown in Fig. 4b is  $\sim 2$  nm. Using the experimental parameters ( $R=2500$  nm,  $k=0.086$  N/m,  $R_{cell}=8.76$   $\mu\text{m}$ ), one has the error in the fitted effective Young's modulus  $E$  of 0.01 kPa (or 0.9% of the modulus value of 1.1 kPa). This error is calculated as one standard deviation of the moduli calculated for five values of the zero-contact uniformly distributed within this 2 nm uncertainty interval. A more solid statistical analysis of the uncertainty of the modulus and other brush layer parameters due to the uncertainty in zero-force will be described in the Results section.

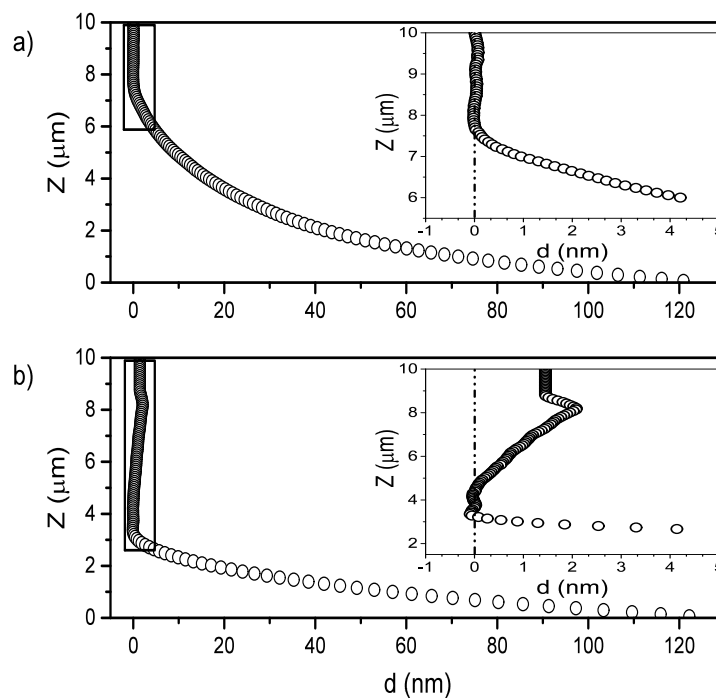


**Figure 4.** Examples of the force curves demonstrating the uncertainty in defining the effective Young's modulus and PB layer parameters when experimentally identifying zero force (zero deflection of the AFM cantilever). (a) A well-defined zero deflection. (b) An uncertain zero deflection; the insert is a zoom version of the curve highlighted by the square box.

Examples of curves obtained on a zebrafish melanocyte cell are shown.

## ***2.2.2. Possible errors due to uncertainty in choosing the fitting region (plateau) of the force-indentation curve to be used for Step 1***

### *2.2.2.1. Location and length of the fitting region*

Step 1 deals with the Hertz fitting of parts of a force-indentation curve, in which the PB layer is almost squeezed. Because the elastic properties of the PB layer and cell body are substantially different, it is impossible to use one simple Hertz fitting for the entire force indentation curves. As was described above, one needs to find the plateau in the dependence of the effective Young's modulus on the indentation force. To do that, one needs to apply the Hertz fitting to different parts of the force indentation curves. There are two degrees of freedom, i.e., uncertainties here: the fitting location and length of the fitting region.

Fig. 5a shows an example of the Hertz fitting for three different locations of the fitting region while keeping the length of the fitted region constant. Extrapolation of the Hertz model beyond the fitting region is shown. One can clearly see that all fitting regions display the extrapolation that diverges significantly from the rest of the curve. For example, the effective Young's modulus  $E$  derived using the region of the force curve located around  $d = 20$  nm is 0.15 kPa, whereas  $E = 1.2$  kPa if the region around  $d = 120$  nm is used for the fitting.

The effect of the change of fitting region length is shown in Fig. 5b. Extrapolations beyond the fitting region are also shown. Similar to Fig. 5a, if the extrapolation curves were the same, it would mean the validity of the applied Hertz model. In the case of the example shown in Fig. 5b, the effective Young's modulus derived from the fitting of the shown 3 fitting regions will be: 0.68, 0.88, 1.2 kPa for regions 1,2,3, respectively.

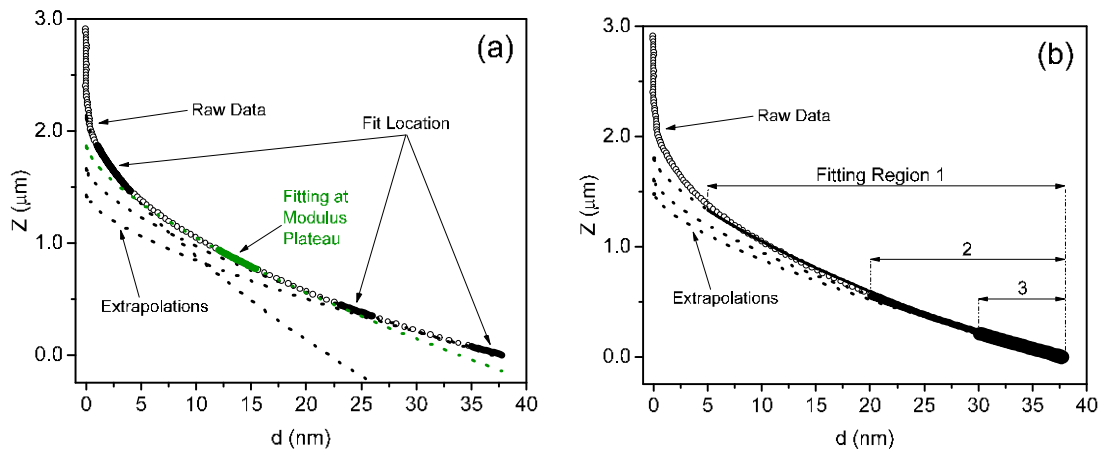


**Figure 5.** An example of the force curve explaining the origin of the uncertainty in defining the effective Young's modulus and PB layer parameters when choosing different fitting regions (Step 1 of the model). Uncertainties in (a) the location and (b) the length of the fitting region. The Hertz extrapolation beyond the fitted region is also shown. The difference in extrapolation beyond the fitted intervals and experimental data demonstrates that the Hertz model could not be applied to the entire indentation curve. Examples of curves obtained on a zebrafish melanocyte cell are shown.

#### 2.2.2.2. Influence of location and length of the fitting region on finding the plateau in the modulus dependence on the indentation force

To find the dependence of the effective Young's modulus on the indentation depth, and correspondingly, the modulus plateau, one should fit the force-indentation curve with the Hertz model for different regions on the indentation force. As was shown in the previous section, this carries an uncertainty due to an arbitrary choice of the length of the fitting region (Fig. 5b).

Figure 6 shows an example of such dependence of the effective Young's modulus calculated for the same force-indentation curve when using different lengths of the fitting region while moving the position of the region along the force curve. It is a bit easier to plot the modulus versus the indentation force rather than that depth (obviously, the depth is proportional to the force). To consider different fitting intervals, it is easier to split the force curve into equal intervals of  $Z$ . Too large  $Z$  intervals excessively smear out the modulus dependence, hiding details of the dependence on the indentation depth. Too small fitting regions produce a rather noisy modulus

dependence. The intermediate fitting regions give a reasonable balance between noise and details.

One can see the plateau in Fig.6 conservatively located in the force interval of 4-5 nN. Although the value of the effective Young's modulus of the plateau is the correct self-consistent results of the Hertz fitting, there is still a relatively small variation of the modulus value within the plateau. For example, if we take the middle size of the fitting region of force ( $\Delta Z = 820$  nm), the modulus changes between  $E = 0.83$  kPa and  $0.86$  kPa within this plateau. This is the error due to uncertainty in choosing the location of the Z interval of the force-indentation curve for calculation of the effective Young's modulus. Note that if the initial plateau point is taken for its corresponding modulus values, then the modulus values for the Z intervals of 410, 615, and 820 would be  $0.89$  kPa,  $0.87$  kPa, and  $0.86$  kPa, respectively. This is the error due to uncertainty in choosing the size of Z interval of the force-indentation curve for the calculation of the effective Young's modulus.

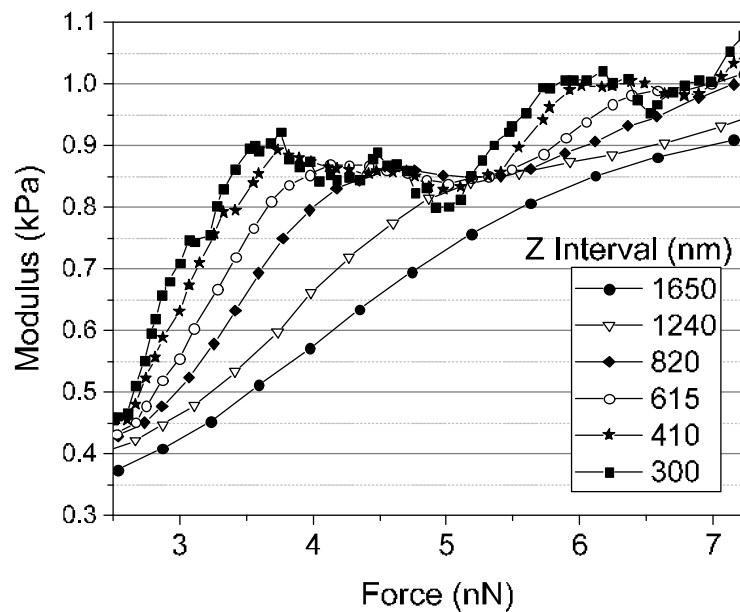


**Figure 6.** An example of the dependence of the effective Young's modulus on the location of Z interval used to calculate the modulus. Several dependences are also shown for different lengths Z interval used to calculate the modulus. One can see that the size of Z interval should not be too large to detect the plateau. Analysis was done on a Zebrafish melanocyte cell.

It is important to note the possible existence of multiple plateaus. In the example of figure 6, one can see that there is another plateau around 6 nN. Because we assume homogeneity of the material, which can only be true for relatively small forces, the Hertz model cannot be used to describe the 2<sup>nd</sup> plateau. It is rather helpful to note that the force of the plateau almost universally stays between 3 to 6 nN for a diversity of cell phenotypes (when using a spherical indentation probe of 5  $\mu\text{m}$ ). Finally, it might be the case in which the plateau does not exist at all. Then, the model cannot be used (cell is presumably too heterogeneous). Fortunately, such a situation is quite rare.

### ***2.2.3. Possible error in the parameters of the pericellular brush layer due to uncertainty in choosing the fitting region in Step 2.***

Step 2 of the model deals with the extraction of the force due to the PB layer. While the extraction of this force using equation (1) is unambiguous, finding the parameters to describe this layer using equation (2) involves two uncertainties similar to the calculation of the modulus, the length, and the location of the fitting region. As previously discussed, the exponential dependence of the indentation force on the separation distance between the AFM probe and cell body (equation (2)) can be seen as a straight line in the force plots when the force is presented in the logarithmic scale. However, due to the natural inhomogeneity of this layer, there are deviations from the pure exponential behavior. Fig. 7 presents two typical examples of the forces due to the PB layer. In Fig. 7a, two chosen fitting regions provide no noticeable variation to the brush parameters of the fit of equation (2), the brush length  $L$  and grafting density  $N$ . The first region corresponds to  $L=1115\text{ nm}$ ,  $N=233\frac{1}{\mu\text{m}^2}$ , and the second region gives  $L=1122\text{ nm}$ ,  $N=229\frac{1}{\mu\text{m}^2}$ . Fig. 6b shows an example of stronger dependence of the brush parameters on the fitting region. The first region corresponds to  $L=1635\text{ nm}$ ,  $N=165\frac{1}{\mu\text{m}^2}$ , whereas the second region gives different values:  $L=1115$ ,  $N=250\frac{1}{\mu\text{m}^2}$ .

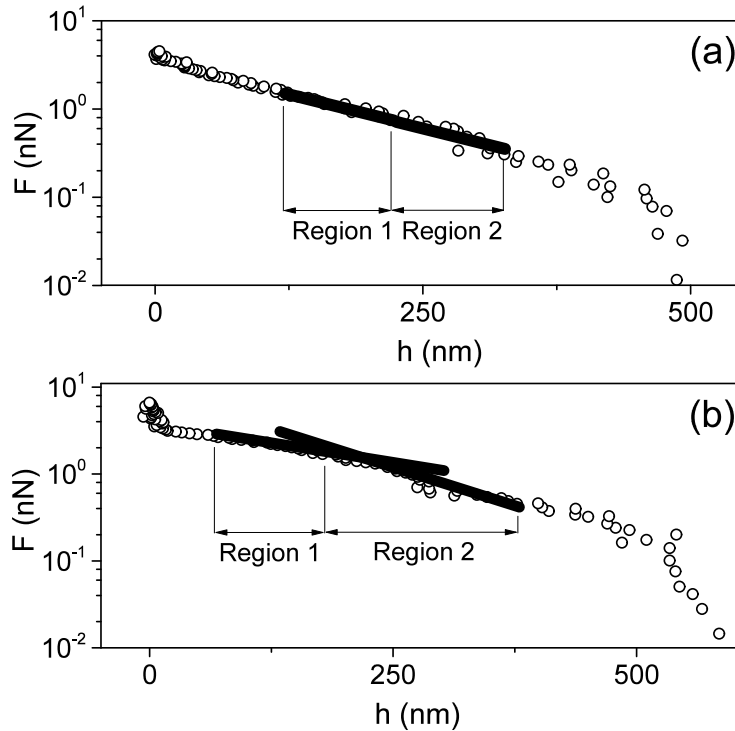


**Figure 7.** Uncertainty because of the freedom in choosing the location of the fitting region in the force due to the PB layer used to calculate the parameter of the PB layer: the brush length and grafting density (Step 2, optional parameterization of the PB layer). (a) A good exponential fitting; no or weak dependence of the brush parameters on the fitting region. (b) A non-ideal exponential fitting; a stronger dependence of the brush parameters on the fitting region. Zebrafish melanocyte cell used for analysis.

Similar to the uncertainty in the fitting region for Step 1, there is uncertainty not only in the choice of location of the fitting region but also in the length of that region. Fig. 8 demonstrates two fitting regions of the force due to the PB layer. The first region corresponds to  $L=1220$  nm,  $N=225 \frac{1}{\mu\text{m}^2}$ , whereas the second region gives different values:  $L=1140$  nm,  $N=235 \frac{1}{\mu\text{m}^2}$ . When we analyze the dependence of these parameters on the fitting region length AND on the location of the fitting region, it is obvious that the larger length of the fitting region gives less variation of the derived brush parameters. In principle, it makes sense to use the full range of allowable size of the fitting region for equation (2),  $0.1 < h/L < 0.8$ .

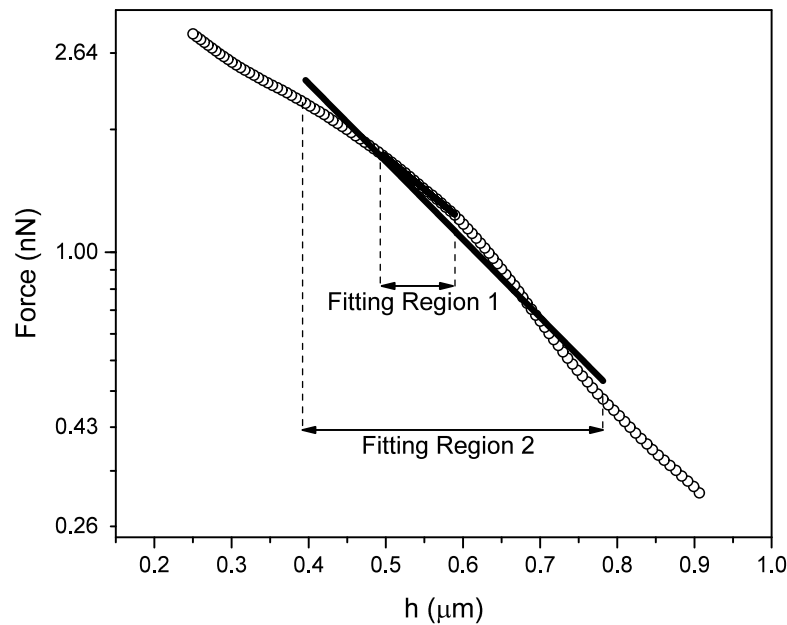


**Figure 8.** Uncertainty due to the freedom in choosing the length of the fitting region to calculate the parameters of the PB layer, the brush length, and grafting density (Step 2, optional parameterization of the PB layer). Zebrafish melanocyte cells were used for analysis.

### 3. Results

Here we present the statistical results for the errors defined in the previous section due to uncertainties in the force curves and model definitions. We analyze the value of the effective Young's modulus of the cell body ( $E$ ), the position of non-deformed cells ( $Z_0$ ), and the parameters of the brush layer: the brush length ( $L$ ) and grafting density ( $N$ ).

#### 3.1. Method of choosing the force curves for analysis and definition of the relative errors

The results were obtained using 60 AFM indentation curves from a diverse source of cells: 20 from zebrafish (melanocytes; 9 cells, about 2 force curves per cell), 20 rats (neuronal cells; 10

cells, about 2 force curves per cell), and 20 humans (cervical cells; 8 cells, about 2 force curves per cell).

To avoid the favorite “pre-filtering” of the force curves chosen for the analysis, we used the following unambiguous rule to pick the force curves. The force curves were chosen *randomly*, spaced over the cell surface when satisfied with the following rules:

1. The location is near the cell top. Since the Hertz model was used to calculate the Young’s modulus, the contact geometry is restricted to sphere-to-sphere contact. This limits the locations of collection of the force curves to either the top of the cell or its flat areas. Many cells did not have flat areas, being relatively small. So, for the sake of uniformity, we restricted the locations only to the top of the cells, similar to the previous publications<sup>17</sup>, when the incline of the cell surface is less than  $10^\circ$ .
2. Only the force curves that demonstrated consistency with the Hertz contact model were considered (otherwise, the concept of the elastic modulus, in general, is not applicable). This was verified by observing the independence of the modulus of the indentation depth (the load force). Specifically, the observed independence/plateau should satisfy the following criteria: a) the plateau size  $> 0.5$  nN, b) the deviation from flatness  $< 10^\circ$  (in kPa vs nN scale).

It is worth noting that the plateau started between 2 – 6 nN for all cells of the study. If the plateau does not occur within this region, then the entire force curve is discounted. It also should be noted that some of the force curves showed multiple plateaus. For consistency with the Hertz model, only the first plateau can be used for calculations.

3. Clearly identifiable zero-force part of the force curve (see, for example, Fig.3). The tolerance of uncertainty was put here to  $< 0.2$  nN (2nm of the cantilever deflection).

For the cell samples used for the analysis in this work, the percent of the force curves chosen around the top of each cell that satisfied the above requirements was as follows: 40% human cervical epithelial cells, 60% rat neurons, and 60% zebrafish fibroblasts.

To find the error / uncertainty in the predicted cell parameters, we calculate the *relative* error, which is independent of the absolute value of the parameter. This is done because it allowed us to compare the errors between different force curves, which may correspond to very

different values of the derived physical parameters. For example, let the average Young's moduli derived from two force curves be 1kPa and 10 kPa, respectively. And let the relative error/uncertainty in the derivation of these moduli be 1% for both curves. It would be rather misleading to try to average the absolute values of the error, 0.1 and 1 kPa in this case. It would lead to a confusing result of 0.5kPa error, which is obviously misleading for the curve that gives 1kPa modules. Because our goal is to present the overall statistics of the error of the model and uncertainty of the experiments, we are saying that the average relative error is 1% in the considered case.

To calculate the relative errors due to the uncertainties described above, we did the following. The Hertz plateau (Fig.6) was defined for a fixed split of the full  $Z$  interval (from the beginning of the contact – the point of first noticeable deflection  $d$  - and the maximum force) into six equal intervals ( $\sim 820$  nm in length for the example of Fig. 6). It corresponds to a reasonable balance between over-smearing and under-smoothing of the modulus dependence on the indentation force.

Errors in the finding of all sought parameters (modulus  $E$ , brush length  $L$ , brush grafting density  $N$ , and non-deformed position of the sample  $Z_o$ ),  $e_m$  are defined as the variance of the sought parameters calculated for each  $m$  force curve:

$$e_m = \frac{100\%}{\bar{x}} \sqrt{\frac{\sum_{i=1}^n (x_i - \bar{x})^2}{n-1}}, \quad (3)$$

where  $x_i$  the values of each parameter calculated within each uncertainty region (e.g., uncertainty in the zero deflection, etc; see Tables 1 – 5),  $n$  is the number of tested points within each uncertainty region ( $n=5$  in this work; the uncertainty regions were analyzed by using five equally distant testing points);  $m=1..20$  for each cell type.

The results of the calculated errors are presented in Tables 1-5 for each analyzed uncertainty. The error due to all uncertainties combined is presented in Table 6. The error averaged on all force curves and one standard deviation are shown in the tables for each of three cell phenotypes.

Overall comparison of absolute values of the analyzed parameters is not within the scope of the present work, we give it for general reference. So the average values of the Young's

modulus of zebrafish fibroblast, rat neurons, and human cervical epithelial cells analyzed in this work were approximately 0.75, 1.6, and 2.7 kPa, respectively. The average effective parameters of the pericellular brush layer, the equilibrium brush length  $L$  and grafting density  $N$  were as follows: 1.9  $\mu\text{m}$  and 170  $\mu\text{m}^{-2}$ , 2.0  $\mu\text{m}$  and 140  $\mu\text{m}^{-2}$ , and 0.93  $\mu\text{m}$  and 170  $\mu\text{m}^{-2}$  for zebrafish fibroblast, rat neurons, and human cervical epithelial cells, respectively.

### 3.2. Errors due to uncertainty in zero deflection of the AFM cantilever

The errors due to uncertainty in zero deflection were calculated as described in section 2.2.1. While the zero deflection was varied within the uncertainty interval, the other tested program parameters were kept constant, specifically:  $Z$  interval (e.g., at 820 nm for the example of Fig. 5); the modulus was taken at the middle of the modulus plateau; the length of the exponential interval was chosen to stay within the exponential force dependence. It was found that the fitting region between 0.1 and 0.4  $h/L$  was always within the exponential force dependence. The location of the exponential interval was taken at the center of the fitting region between 0.1 and 0.4  $h/L$ . The resulting errors calculated as described in the previous section (question 3) are shown in Table 1.

**Table 1.** The error of the brush model parameters due to uncertainty in the zero deflection of the AFM cantilever (the average values and one standard deviation are given).

Cell type	Error in Modulus $E$ %	Error in Brush Length $L$ %	Error in Brush Density $N$ %	Error in $Z_0$ %
Zebrafish Fibroblast	$0.52 \pm 0.32$	$7.2 \pm 3.1$	$6.6 \pm 4.2$	$0.50 \pm 0.26$
Rat Neuron	$0.41 \pm 0.23$	$6.0 \pm 3.3$	$5.3 \pm 3.4$	$0.41 \pm 0.20$
Human Cervical Epithelial	$0.61 \pm 0.30$	$9.8 \pm 3.6$	$7.8 \pm 4.1$	$0.50 \pm 0.24$

### 3.3. Errors due to uncertainty in choosing the fitting region of the force-indentation curve in Step 1

To verify the uncertainty in the modulus due to possible choice of  $Z$  interval (as explained in Section 2.2.2.2 and Fig.5),  $Z$  steps of 300, 410, 615, 820, 1240, and 1650 nm were used ( $Z$  range was divided by  $\sim 16, 12, 8, 6, 4, 3$  equal parts). The modulus plateau was not visible in most curves for step sizes over 820 nm, whereas at step sizes under 410 nm the modulus plateau was excessively noisy. So we used 820, 615, and 410 nm interval lengths and calculated the errors/variation across the modulus plateau. The other tested parameters were kept constant, specifically: zero deflection was taken at the smallest deflection point, the length of the exponential interval was chosen to stay within the exponential force dependence. It was found that the fitting region between 0.1 and 0.4  $h/L$  was always within the exponential force dependence. The location of the exponential interval was taken at the center of the fitting region between 0.1 and 0.4  $h/L$ .

The uncertainty of the modulus within the plateau was found by splitting the plateau into five data points uniformly distributed over the force of the plateau. As the force locations in the plateau were varied, the other tested parameters were kept constant as follows: zero deflection was taken at the smallest deflection point,  $Z$  interval at 615 nm, and the length of the exponential interval was chosen to stay within the exponential force dependence. The location of the exponential interval was taken at the center of the fitting region between 0.1 and 0.4  $h/L$ .

**Table 2.** The error of the brush model parameters due to the length of the fitting region of the force-indentation curve (the average values and one standard deviation are given).

Cell type	Error in Modulus $E$ %	Error in Brush Length $L$ %	Error in Brush Density $N$ %	Error in $Z_0$ %
Zebrafish Fibroblast	$1.9 \pm 0.7$	$2.6 \pm 2.2$	$0.79 \pm 0.86$	$0.7 \pm 0.2$
Rat Neuron	$2.0 \pm 1.2$	$1.7 \pm 1.6$	$0.56 \pm 0.57$	$0.7 \pm 0.4$
Human Cervical Epithelial	$1.3 \pm 0.7$	$2.2 \pm 1.6$	$0.52 \pm 0.62$	$0.5 \pm 0.2$

**Table 3.** The error of the brush model parameters due to the fitting region location of the force-indentation curve (the average values and one standard deviation are given).

Cell type	Error in Modulus $E$ %	Error in Brush Length $L$ %	Error in Brush Density $N$ %	Error in $Z_0$ %
Zebrafish Fibroblast	$1.6 \pm 1.0$	$1.3 \pm 0.9$	$1.1 \pm 0.6$	$0.61 \pm 0.37$
Rat Neuron	$1.4 \pm 0.8$	$0.60 \pm 0.53$	$0.90 \pm 0.53$	$0.56 \pm 0.34$
Human Cervical Epithelial	$1.0 \pm 0.8$	$0.53 \pm 0.36$	$1.1 \pm 0.9$	$0.32 \pm 0.26$

### 3.4. Errors in the parameterization of the pericellular brush layer due to uncertainty in choosing the fitting region in Step 2.

It should be stressed that the extraction of the force due to the PB layer is an unambiguous procedure, which is implemented by using equation 1. However, the parameterization of this force using equation 2 carries the uncertainty described in section 2, the location and length of the interval are to be fitted with equation 2. Thus, in this section, we present the results for the error of parameterization of the PB layer by means of equation 2.

#### 3.4.1. Fitting Interval Location of the Brush

The location of the fitting (exponential) interval was chosen between the allowable limits starting from  $0.1 h/L$  and ending between  $0.4$  and  $0.8 h/L$  (when the force curve was still visually exponential - a straight line in the logarithmic scale). The interval locations were chosen by equally dividing the fitting interval into five equal sub-intervals. Note that as the fitting region location was varied, the other tested model parameters were kept constant, specifically: zero deflection taken at the smallest deflection point,  $Z$  interval as  $615$  nm, the modulus value within the middle of the visible modulus plateau.

**Table 4.** The error of parameterization of the PB layer due to uncertainty in the location of the fitting region (the average values and one standard deviation are given).

<b>Cell type</b>	<b>Error in Brush Length, L %</b>	<b>Error in Brush Density, N %</b>
Zebrafish Fibroblast	17 ± 10	25 ± 15
Rat Neuron	14 ± 8.7	22 ± 11
Human Cervical Epithelial	17 ± 7.6	25 ± 11

### 3.4.2. Fitting Interval Length of the Brush

The length of the exponential interval was varied between the maximum and minimum ones divided by a factor of 1,2,3,4,5. The maximum length of the exponential interval was the length of the interval starting from 0.1 h/L and ending between 0.4 and 0.8 h/L (when the force curve was still visually exponential, a straight line in the logarithmic scale). The minimum length of the exponential interval was 1/10<sup>th</sup> of the maximum one.

Note that as the fitting region length was varied, the other tested model parameters were kept constant, specifically: zero deflection taken at the smallest deflection point, Z interval at 615 nm, the modulus point at the middle of the visible modulus plateau, and the location of the exponential interval was taken at the center of the fitting region between 0.1 and 0.4 h/L.

**Table 5.** The error of parameterization of the PB layer due to uncertainty in the length of the fitting region (the average values and one standard deviation are given).

<b>Cell type</b>	<b>Error in Brush Length, L %</b>	<b>Error in Brush Density, N %</b>
Zebrafish Fibroblast	6.3 ± 5.7	9.2 ± 8.4
Rat Neuron	4.6 ± 3.1	7.8 ± 5.7
Human Cervical Epithelial	5.1 ± 3.3	8.4 ± 6.0

## 4. Discussion

As was described, the brush model consists of two almost independent parts: calculation of the effective Young's modulus of the cell body (Step 1) and the extraction of the force-due-to-brush (Step 2). The uncertainties (or errors) in the derivation of both parts due to ambiguity in the interpretation of experimental data and the model steps were presented in Tables 1-3. Additional Tables 4 and 5 show the results of ideologically different analysis, which is a part of Step 2, the uncertainties or errors in the parameterization of the force-due-to-brush by using the exponential formula, equation (2). The difference between the brush layer data presented in Tables 1-3 and 4,5 is as follows. Tables 1-3 show the ambiguity in the derived force-due-to-brush while keeping the uncertainties in the parameterization of the brush fixed, whereas Tables 4,5 describe the deviation of the force-due-to-brush from the exponential law. Thus, we discuss the results of these tables separately.

Tables 1-3 present the errors/uncertainties in the calculation of the output model parameters: the effective Young's modulus ( $E$ ) and undeformed position ( $Z_0$ ) of the cell body, and the force-due-to-brush parameterized with a fixed fitting interval and the middle position of the fitting interval. As one can see, all these errors are sufficiently small, in particular, the error of defining the modulus and the undeformed position. It gives us justification to analyze the sources of the errors separately. The error of each output parameter  $P^{out}$  can be represented as a function of some input parameters  $\{P_1^{in}, P_2^{in}, \dots, P_N^{in}\}$ , which are defined with some uncertainty  $\{\delta P_1^{in}, \delta P_2^{in}, \dots, \delta P_N^{in}\}$ . (The specific examples of input parameters are the ones defined in section 2.2.) Then, the total error/uncertainty of the output parameter  $P^{out}$  can be found as follows:

$$\delta P^{out} = \frac{\partial P^{out}}{\partial P_1^{in}} \delta P_1^{in} + \frac{\partial P^{out}}{\partial P_2^{in}} \delta P_2^{in} + \frac{\partial P^{out}}{\partial P_N^{in}} \delta P_N^{in} + O(\delta P_1^{in}, \delta P_2^{in}, \dots, \delta P_N^{in})^2 \quad (4)$$

Due to a relatively small errors, we can keep only the linear terms in this formula. It should be noted that a potential cross-correlation between different sources of the uncertainties discussed in this work may exist. However, being the second-order effects, they can be ignored. Adding the errors described in tables 1-3 together (linear contributions in equation 4), one

obtains the results presented in Table 6. One can see that overall errors are rather reasonable and well within the typical uncertainty in the spring constant of the AFM cantilever ( $\sim 5\text{-}20\%$ ).<sup>49-51</sup>

**Table 6.** The total error of the brush model parameters due to 1) uncertainty in the zero deflection of the AFM cantilever, 2) the length of the fitting region of the force-indentation curve, and 3) the fitting region location of the force-indentation curve. The average values of the errors (calculated using equation 3) and one standard deviation are given.

Cell type	Error in Modulus $E$ %	Error in Brush Length $L$ %	Error in Brush Density $N$ %	Error in $Z_0$ %
Zebrafish Fibroblast	4.0	11	8.5	1.8
Rat Neuron	3.8	8.3	6.8	1.7
Human Cervical Epithelial	2.9	13	9.4	1.3

Now, let us discuss the deviation of the force-due-to-brush from the exponential law, which is shown in Tables 4,5. One can see that the uncertainty due to the position of the fitting interval can be quite substantial, whereas the dependence on the length of the fitting interval is much smaller. As we already briefly mentioned, this is NOT the error of the model but rather an indication of deviation of the behavior of the actual pericellular brush layer from an entropic brush model given by equation 2. This should not be a surprise because the entropic brush model is obviously an oversimplification of the actual pericellular layer. As was demonstrated, the pericellular layer may consist of two different constituents, a molecular part (glycoproteins and glycosaccharides) and corrugation of the membrane (microridges, microvilli, and in some cases, cilia and filopodia). The detailed analysis of the deviations of the force due to brush from the exponential law is beyond the scope of the present work. It should be noted, though, that these deviations can be used for additional characterization of the pericellular brush layer. This will be done in future works.

It is instructional to discuss the rule of selection of the force curves as well as the total number of the force curves analyzed in this work. In general, it is tempting to apply some

computer algorithm or machine learning analysis to prescreen the curves suitable for AFM analysis. Technically, it can definitely be done. However, it would not bring any noticeable enhancement of the method described in this paper. The reason for that is that the total number of force curves to analyze in a typical cell indentations experiment by means of AFM is relatively small. The cell indentation is usually done with a load speed  $< 10 \mu\text{m/s}$  to avoid a too large viscoelastic response of the cell material, and at the same time, not to disturb the cell too much during an excessively long experiment. Next, to avoid the nonlinear overstretching of cells<sup>4,32</sup>, the indentation experiments are done with the AFM probe with a micron radius of curvature. Furthermore, as we mentioned before, one needs to collect the force curves only above the cell top (or on a flat area if it exists). All this results in a rather limited number of force curves that can be used to extract geometry- and experiment- independent values of cell parameters in a self-consistent way. Typically, the number of suitable force curves rarely exceeds 10 per cell. Finally, simple algorithms like the goodness of curve fitting ( $R^2$  or chi-square) do not bring any noticeable separation between good and bad force curves (unless the curve is really bad, meaning it doesn't look like force curves all). Thus, it seems to be premature to develop a special algorithm to filter out force curves that are not suitable for the analysis through the brush model.

As the total number of the force curves analyzed in this work (~120 were screened through the rules described in section 3.1, and 60 were found to be good for the numerical analysis), it looks to be sufficient because of consistent results across all force curves. This can be seen through a relatively small standard deviation of the obtained errors, as well as consistency between the different cell phenotypes.

In conclusion, the brush model proves to be robust. The obtained errors due to the model and experimental uncertainties typically are less than 10%. The uncertainty in the definition of the modulus of the cell body (the effective Young's modulus) is less than 4%. This is comparable or smaller than the uncertainty that may come from the measurements of the spring constant of the AFM cantilever (5-20%)<sup>4,32,42</sup>.

## Experimental Methods

### *Cells*

AFM force-indentation curves were collected on three distinct cell types as described in detail in corresponding references: zebrafish fibroblast<sup>52</sup>, rat neuron<sup>6</sup>, and human cervical epithelial samples<sup>17,53</sup>. Here we briefly describe the methods of sample preparation to outline details of specific cell preparation for each cell type. Zebrafish fibroblast samples contained both dormant and cancer-initiating cells, and were analyzed at 21°C. Rat neuron samples contained normal cells that were analyzed at 25°C and 37°C. Human cervical epithelial samples contained normal cells analyzed at 21°C. All cells adhered tightly to the bottom of 60 mm cell culture dishes. The dishes were mounted on the chuck of the AFM with a double sticky tape. All indentation experiments were done on living cells in their specific medium.

### *Zebrafish fibroblast cells*

After humane euthanasia of the zebrafish, a spontaneously arising crestin: GFP + melanoma tumor with some adjacent melanocytes was excised with a scalpel and dissociated mechanically with a razor blade followed by treatment with 50% Ham's F12/50% DMEM, 10× Pen/Strep, 0.075 mg/mL Liberase for 30 minutes. The reaction was stopped with 50% Ham's F12/50% DMEM, 10× Pen/Strep, 15% heat-inactivated fetal calf serum. After filtering through a 40-micron mesh filter, cells were plated on a 60 mm plastic petri dish coated with fibronectin and grown in zebrafish complete medium until imaging. Right before imaging, cells were washed with PBS buffer, and studied with AFM in fresh PBS solution.

### *Human cervical epithelial cells*

The cells were prepared by a two-stage enzymatic digestion of cervical tissue as described [33] and cells were maintained in keratinocyte serum-free medium (Invitrogen, Carlsbad, CA). Serum-free media do not have inevitable variability of sera, and it suppress a possible growth of fibroblasts. Cervical epithelial tissues were isolated from healthy tissues of endzone of cervix as described in<sup>54</sup>. All donor tissues were obtained from the Cooperative Human Tissue Network. The obtained normal cervical cells were used between 40 to 60 population doublings. All

scanning and measurements related to rigidity were performed on viable cells maintained to room temperature in Hank's balanced salt solution (HBSS) within 2-3 hours after removal of the growth medium.

### *Rat neurons*

Rat cortices were obtained from Tufts Medical School isolated from embryonic day 18 rats. The isolated cortices were incubated at 37°C in 5 mL of trypsin for 20 minutes. Trypsin was inhibited with 10 mL of neurobasal medium (Life Technologies, Frederick, MD) which was supplemented with GlutaMAX, b27 (Life Technologies), pen/strep (Life Technologies) 1%, and 10 mg of soybean trypsin inhibitor (Life Technologies). The cortices were mechanically dissociated, the cells were centrifuged, the supernatant removed, and the cells were re-suspended in 20 mL of neurobasal medium with L-glutamate (Sigma-Aldrich, St. Louis, MO). Cortices were incubated in serum-free media, which reduces glia proliferation. The cells were mechanically re-dispersed, counted, and plated at a density of 250,000 cells per 3.5 cm culture disk. Each sample of cells was grown in 5% CO<sub>2</sub> at 37°C for a minimum of 2 days before measurements. Neuronal cells were optically selected based on morphology.

Cell samples were cultured on 3.5 cm glass disks manufactured to fit in the Asylum Research Bioheater fluid cell (Asylum Research, Santa Barbara, CA). Poly-D-lysine (PDL) (Sigma-Aldrich, St. Louis, MO) coating was added to the glass disks by immersing them in a PDL solution (0.1 mg/ml) for 2 hours at room temperature.

### *Atomic force microscopy*

A Nanoscope™ Dimension 3100 (Digital Instruments/Veeco, Inc., Santa Barbara, CA) atomic force microscope (AFM) was used to obtain the data on human cervical epithelial cells. Zebrafish fibroblasts were studied with BioScope Catalyst (by Bruker Nano, Inc., Santa Barbara, CA). MFP-3D-Bio AFM (Asylum Research/Oxford Instruments, Santa Barbara, CA) was used to study rat neurons. Standard cantilever holders for operation in liquids were employed. All AFM cantilevers used in this study had 5-13 micron spherical probes attached to tipless cantilevers of 0.01-0.1 N/m spring constant. To obtain the distribution of the interface properties of the cell, the force-volume mode of operation was utilized. The force volume mode provides

information about both the surface topography and the force curves simultaneously. This is important because the models to quantify the measurements have been developed for a sphere over a surface of known geometry, a plane. Thus, we processed force curves only over relatively flat areas of the cells ( $<10^\circ$  of inclination angle). The force curves were collected over areas of several hundred square microns with the vertical ramp size within 4-5  $\mu\text{m}$ . The AFM probe moves up and down during the force collection with a frequency of 2Hz to decrease viscoelastic effects to a reasonable minimum (the approach speed was  $\sim 10 \mu\text{m/s}$  for all samples). While we could not avoid the viscoelastic effects completely, to be consistent, we performed all measurements with the same oscillation frequency of 2Hz. The global position of the AFM probe was controlled by the built-in video system, which allows observation of areas from  $150 \times 110$  to  $675 \times 510 \mu\text{m}^2$  with  $1.5\mu\text{m}$  resolution. The measurement methodology described in detail can be found, for example, in ref. <sup>55</sup>.

## **ACKNOWLEDGMENTS**

Support of this work from the National Science Foundation is acknowledged by I.S. (CMMI 1435655, CMMI 1937373).

## **COMPETING FINANCIAL INTERESTS**

The authors declare no conflict of interest.

**REFERENCES**

1. C. L. Essmann, M. Elmi, M. Shaw, G. M. Anand, V. M. Pawar and M. A. Srinivasan, *Nanomedicine*, 2017, **13**, 183-189.
2. I. Sokolov, M. Firtel and G. S. Henderson, *Journal of Vac.Sci.&Tech. B*, 1996, **14**, 674-678.
3. M. Stark, C. Moller, D. J. Muller and R. Guckenberger, *Biophys J*, 2001, **80**, 3009-3018.
4. P. H. Wu, D. R. B. Aroush, A. Asnacios, W. C. Chen, M. E. Dokukin, B. L. Doss, P. Durand-Smet, A. Ekpenyong, J. Guck, N. V. Guz, P. A. Janmey, J. S. H. Lee, N. M. Moore, A. Ott, Y. C. Poh, R. Ros, M. Sander, I. Sokolov, J. R. Staunton, N. Wang, G. Whyte and D. Wirtz, *Nature Methods*, 2018, **15**, 491-498.
5. I. Sokolov and M. E. Dokukin, *Methods Mol Biol*, 2018, **1814**, 449-468.
6. M. Simon, M. Dokukin, V. Kalaparathi, E. Spedden, I. Sokolov and C. Staii, *Langmuir*, 2016, **32**, 1111-1119.
7. C. G. Galbraith and M. P. Sheetz, *Current Opinion in Cell Biology*, 1998, **10**, 566-571.
8. V. Vogel and M. Sheetz, *Nature Reviews Molecular Cell Biology*, 2006, **7**, 265-275.
9. O. Chaudhuri and D. J. Mooney, *Nature Materials*, **11**, 568-569.
10. S. Suresh, *Acta Biomaterialia*, 2007, **3**, 413-438.
11. S. E. Cross, Y. S. Jin, J. Rao and J. K. Gimzewski, *Nature Nanotechnology*, 2007, **2**, 780-783.
12. I. Sokolov, S. Iyer and C. D. Woodworth, *Nanomedicine: Nanotechnology, Biology and Medicine (Nanomedicine)*, 2006, **2**, 31–36.
13. G. B. Nash, E. O'Brien, E. C. Gordon-Smith and J. A. Dormandy, *Blood*, 1989, **74**, 855-861.
14. J. Li, M. Dao, C. T. Lim and S. Suresh, *Biophys J*, 2005, **88**, 3707-3719.
15. M. J. Paszek, N. Zahir, K. R. Johnson, J. N. Lakins, G. I. Rozenberg, A. Gefen, C. A. Reinhart-King, S. S. Margulies, M. Dembo, D. Boettiger, D. A. Hammer and V. M. Weaver, *Cancer Cell*, 2005, **8**, 241-254.
16. M. Lekka and P. Laidler, *Nat Nanotechnol*, 2009, **4**, 72; author reply 72-73.
17. I. Sokolov, M. E. Dokukin and N. V. Guz, *Methods*, 2013, **60**, 202-213.
18. I. Sokolov, S. Iyer, V. Subba-Rao, R. M. Gaikwad and C. D. Woodworth, *Applied Physics Letters*, 2007, **91**, 023902-023901-023903.

19. H. Oberleithner, M. Walte and K. Kusche-Vihrog, *Front Physiol*, 2015, **6**.
20. D. G. Warnock, K. Kusche-Vihrog, A. Tarjus, S. Sheng, H. Oberleithner, T. R. Kleyman and F. Jaisser, *Nat Rev Nephrol*, 2014, **10**, 146-157.
21. M. J. Paszek, C. C. DuFort, O. Rossier, R. Bainer, J. K. Mouw, K. Godula, J. E. Hudak, J. N. Lakins, A. C. Wijekoon, L. Cassereau, M. G. Rubashkin, M. J. Magbanua, K. S. Thorn, M. W. Davidson, H. S. Rugo, J. W. Park, D. A. Hammer, G. Giannone, C. R. Bertozzi and V. M. Weaver, *Nature*, 2014, **511**, 319-325.
22. E. L. Baker, R. T. Bonnecaze and M. H. Zaman, *Biophys J*, 2009, **97**, 1013-1021.
23. E. C. Woods, F. Kai, J. M. Barnes, K. Pedram, M. W. Pickup, M. J. Hollander, V. M. Weaver and C. R. Bertozzi, *Elife*, 2017, **6**.
24. D. Gonzalez-Rodriguez, K. Guevorkian, S. Douezan and F. Brochard-Wyart, *Science*, 2012, **338**, 910-917.
25. S. Iyer, R. M. Gaikwad, V. Subba-Rao, C. D. Woodworth and I. Sokolov, *Nature Nanotechnology*, 2009, **4**, 389-393.
26. N. V. Guz, M. E. Dokukin, C. D. Woodworth, A. Cardin and I. Sokolov, *Nanomedicine*, 2015, **11**, 1667-1675.
27. M. E. Dokukin, N. V. Guz, C. D. Woodworth and I. Sokolov, *New J Phys*, 2015, **17**, 033019
28. M. E. Dokukin, N. V. Guz, R. M. Gaikwad, C. D. Woodworth and I. Sokolov, *Physical Review Letters*, 2011, **107**, 028101.
29. I. Sokolov, *Future Oncology*, 2015, **11**, 3049-3051.
30. I. Sokolov, M. E. Dokukin, V. Kalaparathi, M. Miljkovic, A. Wang, J. D. Seigne, P. Grivas and E. Demidenko, *Proceedings of the National Academy of Sciences of the United States of America*, 2018, **115**, 12920-12925.
31. Siona Prasad, Alex Rankine, Tarun Prasad, Patrick Song, Maxim E. Dokukin, Nadezda Makarova, Vadim Backman, Igor Sokolov, "Atomic Force Microscopy Detects the difference in Cancer Cells of different Neoplastic Aggressiveness via Machine Learning", *Advanced NanoBiomed Research*, 1, 2000116, 2021
32. N. Guz, M. Dokukin, V. Kalaparathi and I. Sokolov, *Biophysical Journal*, 2014, **107**, 564-575.
33. Y. Ding, G. K. Xu and G. F. Wang, *Scientific reports*, 2017, **7**.

34. M. E. Dokukin, H. Kuroki, S. Minko and I. Sokolov, *Macromolecules*, 2017, **50**, 275-282.
35. M. Dokukin, Y. Ablaeva, V. Kalaparathi, A. Seluanov, V. Gorbunova and I. Sokolov, *Biophysical Journal*, 2016, **111**, 236-246.
36. M. E. Dokukin, N. V. Guz and I. Sokolov, *Jpn J Appl Phys*, 2017, **56**, 08LB01.
37. M. Targosz-Korecka, M. Jaglarz, K. E. Malek-Zietek, A. Gregorius, A. Zakrzewska, B. Sitek, Z. Rajfur, S. Chlopicki and M. Szymonski, *Scientific reports*, 2017, **7**, 15951.
38. J. W. Nicholatos, T. M. Robinette, S. V. P. Tata, J. D. Yordy, A. B. Francisco, M. Platov, T. K. Yeh, O. R. Ilkayeva, F. K. Huynh, M. Dokukin, D. Volkov, M. A. Weinstein, A. R. Boyko, R. A. Miller, I. Sokolov, M. D. Hirschey and S. Libert, *Geroscience*, 2019, DOI: 10.1007/s11357-019-00062-6.
39. N. Gavara, *Scientific reports*, 2016, **6**, 21267.
40. M. Kopycinska-Muller, R. H. Geiss and D. C. Hurley, *Ultramicroscopy*, 2006, **106**, 466-474.
41. R. Wagner, R. Moon, J. Pratt, G. Shaw and A. Raman, *Nanotechnology*, 2011, **22**.
42. Z. C. Ying, M. G. Reitsma and R. S. Gates, *Review of Scientific Instruments*, 2007, **78**.
43. M. E. Dokukin, N. V. Guz and I. Sokolov, *Biophys J*, 2013, **104**, 2123-2131.
44. I. Sokolov and M. E. Dokukin, *Nanoscale Imaging: Methods and Protocols*, 2018, **1814**, 449-468.
45. M. E. Dokukin and I. Sokolov, *Macromolecules*, 2012, **45**, 4277-4288.
46. H. R. Hertz, *Journal*, 1882, **1882**, 156.
47. H. J. Butt, M. Kappl, H. Mueller, R. Raiteri, W. Meyer and J. Ruhe, *Langmuir*, 1999, **15**, 2559-2565.
48. S. Iyer, R. M. Gaikwad, V. Subba-Rao, C. D. Woodworth and I. Sokolov, *Nature Nanotechnology*, 2009, **4**, 389-393.
49. R. S. Gates, W. A. Osborn and J. R. Pratt, *Nanotechnology*, 2013, **24**.
50. G. A. Matei, E. J. Thoreson, J. R. Pratt, D. B. Newell and N. A. Burnham, *Review of Scientific Instruments*, 2006, **77**.
51. M. L. B. Palacio and B. Bhushan, *Nanotribology and Nanomechanics: Measurement Techniques and Nanomechanics, Vol 1*, 2011, DOI: 10.1007/978-3-642-15283-2\_4, 135-193.

52. N. Makarova, V. Kalaparthi, A. Wang, C. Williams, M. E. Dokukin, C. K. Kaufman, L. Zon and I. Sokolov, *J Mech Behav Biomed*, 2020, **107**, 103746.
53. I. Sokolov, S. Iyer, V. Subba-Rao, R. M. Gaikwad and C. D. Woodworth, *Applied Physics Letters*, 2007, **91**.
54. C. D. Woodworth, J. Doniger and J. A. Dipaolo, *J. Virol.*, 1989, **63**, 159-164.
55. I. Sokolov, in *Cancer Nanotechnology – Nanomaterials for Cancer Diagnosis and Therapy*, eds. H. S. Nalwa and T. Webster, ASP, 2007.